Strong-coupling effective-field theory for asymmetrically charged plates with counterions only

Ladislav Šamaj,[1,2] Emmanuel Trizac,[2,3] and Martin Trulsson[4]
[1]*Institute of Physics, Slovak Academy of Sciences, Dúbravská cesta 9, 84511 Bratislava, Slovakia*
[2]*LPTMS, Université Paris-Saclay, CNRS, 91405 Orsay, France*
[3]*ENS de Lyon, 46 allée d'Italie, 69364 Lyon, France*
[4]*Computational Chemistry, Lund University, SE-221 00 Lund, Sweden*

(Received 21 February 2024; accepted 27 June 2024; published 30 July 2024)

We are interested in rationalizing the phenomenon of like-charge attraction between charged bodies, such as a pair of colloids, in the strong coupling regime. The two colloids are modelled as uniformly charged parallel plates, neutralized by mobile counterions. In an earlier work [Palaia *et al.*, J. Phys. Chem. B **126**, 3143 (2022)], we developed an effective-field theory for symmetric plates, stemming from the ground-state description that holds at infinite couplings. Here, we generalize the approach to the asymmetric case, where the plates bear charges of the same sign, but of different values. In the symmetric situation, the mobile ions, which are localized in the vicinity of the two plates, share equally between both of them. Here, the sharing is nontrivial, depending both on the coupling parameter and the distance between the plates. We thus introduce a counterion occupation parameter that is determined variationally to ensure minimum of the free energy. The analytical results for the pressure as a function of the plate-plate distance d agree well with our Monte Carlo data, in a large interval of strong and intermediate coupling constants Ξ. We show in particular that within this description there exists a range of large distances at which the attractive pressure features a $1/d^2$ behavior.

DOI: 10.1103/PhysRevE.110.014609

I. INTRODUCTION

Mesoscopic bodies (macroions or colloids), immersed in a polar solvent like water, release from their surfaces (due to efficient solvation) mobile "counterions." Ions in Coulomb fluids are generically of both signs, however, one can reach experimentally the limit of deionized (salt-free) suspensions with no "coions" [1–3]. The curved surface of the large colloid is usually approximated by a planar surface and the modulated charge density fixed on colloid's surfaces by the uniform one. Counterions in the vicinity of a charged colloid form an electric double layer (EDL) [4–6]. The study of the effective interaction between two like-charged EDLs, mediated by counterions, is of special experimental and theoretical interest in many branches of physics, chemistry and biochemistry [7–11].

Like-charged macroions always repel one another in the high-temperature (weak coupling, WC) regime described by the mean-field Poisson-Boltzmann (PB) theory [12–16] as well as its functional improvement via a loop expansion [17–19].

At low enough temperatures, i.e., in the strong-coupling (SC) regime, a counterintuitive attraction of like-charged macromolecules was observed by computer simulations [20–22] as well as experimentally [23–27]. Different theoretical treatments have been proposed for the SC regime. In the virial SC approaches [28–30], the leading SC term of the counterion density corresponds to a single particle theory in the electric potential of charged wall(s); resulting densities have been confirmed by Monte Carlo (MC) simulations [28,29,31–33]. Next correction orders in inverse powers of the coupling constant, obtained within a virial fugacity expansion, require a renormalization of infrared divergencies; comparison with MC simulations shows that the first correction term has the correct functional form in space, but an incorrect prefactor. Another type of SC theories was based on the classical Wigner crystal of counterions created on the wall surfaces at zero temperature [11,34,35]. A harmonic analysis of counterion deviations from their ground-state Wigner positions [36,37] reproduces correctly the leading single-particle picture of the virial SC approach. The first correction term to the counterion density is in excellent agreement with MC data for strong as well as intermediate Coulombic couplings. To adapt the Wigner SC approach to the fluid phase, the Wigner structure was substituted by a correlation hole (i.e., the depletion region around a charge due to Coulomb repulsion of the same charges) in Refs. [38,39].

For two parallel symmetrically charged planar surfaces, it was recently shown [40] that the relevant physics for the like-charge attraction is the ground-state one. The method [40] is based on the introduction of effective fields which reflect the partial screening of the electric field induced by the fixed surface charge density of a plate by counterion layers. According to Earnshaw's theorem [41], in the ground-state counterions stick to the surfaces of the confining plates. Upon changing the distance between plates from 0 to ∞, a sequence of five Wigner phases I–V emerges at zero temperature [42–47]. These staggered phases consist of two equivalent lattice structures on the left and right plates, shifted with respect to one another by a half period in both spatial directions. Since each plate as a whole (i.e., the surface charge density plus the corresponding counterions) is electroneutral, the effective interaction between the walls is short-ranged (exponentially decaying) at large distances. The extension of the

ground-state effective fields to nonzero temperatures leads to a formula for the pressure which interpolates between the "ideal gas" regime for small inter-plate distances and the "Wigner" regime at large distances. The pressure fulfills known exact requirements and its dependence on the inter-plate distance is in a perfect agreement with MC data, in a large interval of strong and intermediate values of the coupling constant.

The aim of this paper is to extend the effective-field method [40] to asymmetric parallel plates; throughout this paper, asymmetrically charged plates refers to surfaces with unequal but same-sign surface charge densities. The ground state of asymmetric plates was studied by using analytical and computational evolutionary techniques [48,49], as well as unsupervised learning [50]. In comparison with the symmetrically charged plates, the asymmetric system exhibits much more phases, sometimes of exotic nature (pentagonal, snub square, etc.). Each plate as a whole (i.e., the surface charge of the plate plus the counterions attached to that plate) is, in general, not neutral which implies a long-ranged (inverse-power law) effective interaction between the plates at large distances between them. This nonneutrality phenomenon complicates substantially the analytic treatment of the asymmetric problem because of the presence of an additional free parameter into the theory, namely the one related to the counterion occupations of the plates. In the ground state, this parameter is determined variationally to ensure minimum of the ground-state energy. In this paper, we go to nonzero-temperature and construct the free energy of the system in the strong-coupling regime, in terms of deviations of counterions from their ground-state positions. The counterion occupation parameter is determined variationally to ensure minimum of the free energy. Applying then the effective-field idea [40], analytic results for the pressure as a function of the distance d between the plates agree very well with our MC data in a large interval of strong and intermediate coupling constants. For large enough distances d of the *attractive* regime, the pressure is shown to scale like $1/d^2$, with the nonuniversal prefactor which carries the structural information about the Wigner ground state and depends on the asymmetry parameter of the plates. We stress that at asymptotically large distances, the pressure is expected to follow the Poisson-Boltzmann behavior, and to be repulsive there, decaying as $1/d^2$.

The paper is organized as follows. Section II brings basic setup for the asymmetric model, together with the notation used. The ground-state structures for symmetrically and asymmetrically charged plates are summarized in Sec. III. The emphasis is put on the regions of small and large interplate distances characterized by a few notable bilayer phases. Although Secs. II and III summarize in a relatively detailed way the known results from previous papers, they make the presentation self-contained. The presented formulas are crucial for a clear understanding of original results derived in the succeeding sections and help the potential reader to reproduce the obtained analytic results. Section IV concerns the analytic effective-field treatment of the asymmetric model at nonzero temperatures, within the SC regime. The pressure is obtained from either the contact value theorem (Sec. IV A) or the thermodynamic route (Sec. IV B). Details of MC simulations performed in this paper are described in Sec. V. The comparison of the analytic and MC results for intermediate values of the coupling constant $\Xi = 30, 100$ is made in Sec. VI. The emphasis is put on both the small-distance region, where the attractive pressure exhibits its minimum, as well as large-distance region, where the attractive pressure exhibits the $1/d^2$ decay with a nonuniversal prefactor. Section VII is a short recapitulation, together with some concluding remarks.

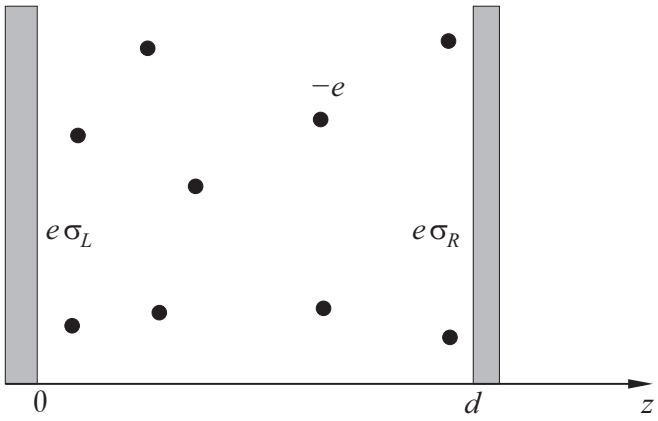

FIG. 1. The geometry (along the z axis) of two parallel walls at distance d. There is a homogeneous surface charge density $e\sigma_L$ fixed on the left wall and $e\sigma_R$ on the right wall. The pointlike counterions of charge $-e$, moving freely between the walls, are pictured as black circles.

II. BASIC SETUP FOR THE ASYMMETRIC MODEL

A. Notation

Let us consider a pair of parallel plates at distance d, in the three-dimensional (3D) Cartesian space of points $\mathbf{r} = (x, y, z)$; see Fig. 1. The left and right plates of the same (large) surface S spread along the two-dimensional (2D) plane (x, y), their positions along the perpendicular z axis being 0 and d, respectively. The left (right) plate carries a homogeneous surface charge density $e\sigma_L$ ($e\sigma_R$) where e is the elementary charge. Colloids acquire, in most cases, their charge from a chemical equilibrium, of, e.g., ions or charged molecules, between their surface and the solution medium; this equilibrium depends, in general, on the thermodynamic parameters [15,16]. The investigation of the surface charge regulation, where σ_R and σ_L would no longer be constant, goes beyond the scope of this work. We note that some surfaces like mica are structural and cannot change their charge density; this includes a number of mineral surfaces. For titratable surfaces the surface charge would indeed vary, but this relies also on a salt reservoir which we do not allow for. Nevertheless, in the most frequent common chemical equilibrium when the solution's pH is far away from the colloid's pKa values, the colloid can essentially be regarded as having a fixed surface charge.

There are N classical counterions with charge say of unit valence $-e$ which move in the space between the plates $\Lambda = \{\mathbf{r}, 0 < z < d\}$. The requirement of the overall neutrality reads

$$N = (\sigma_L + \sigma_R)S. \tag{2.1}$$

The counterions are considered to be pointlike. This simplification is suitable especially for low temperatures when

counterions maximize their separation within the counterion layer and their size will be irrelevant up to the spacing of the counterion structure [51].

Without any loss of generality one can assume that $\sigma_L > 0$. Rescaling appropriately the model's parameters, it is sufficient to consider the asymmetry parameter

$$A = \frac{\sigma_R}{\sigma_L} \tag{2.2}$$

inside the interval $[-1, 1]$; the limiting value $A = -1$ corresponds to the trivial case $\sigma_R = -\sigma_L$ with no counterions between the plates, $A = 1$ corresponds to the symmetrically charged plates $\sigma_L = \sigma_R$. Likely charged asymmetric plates with

$$0 < \sigma_R < \sigma_L, \tag{2.3}$$

i.e., $A \in (0, 1)$, are of special interest. Let the dielectric constant of the walls ε_W be the same as that of the medium the counterions are immersed in ε, $\varepsilon_W = \varepsilon$, i.e., there are no image charges. The vacuum $\varepsilon = 1$ is taken for simplicity, again without loss of generality. The system is considered either at zero temperature $T = 0$ or in thermal equilibrium at nonzero temperatures $T > 0$.

B. Zero temperature, $T = 0$

In the ground state ($T = 0$), according to Earnshaw's theorem [41], the Coulomb charges are expelled from the slab interior and stick to the surfaces of the confining plates. In particular, N_L (N_R) counterions collapse on the left (right) plate surfaces, $N = N_L + N_R$ and organize themselves onto certain left (right) crystal structures. The densities of counterions at the surfaces of the plates are given by

$$n_L = \frac{N_L}{S}, \quad n_R = \frac{N_R}{S}. \tag{2.4}$$

According to the overall electroneutrality condition (2.1), the counterion densities at plates are constrained by

$$n_L + n_R = \sigma_L + \sigma_R. \tag{2.5}$$

It is useful to introduce the (occupation) order parameter

$$p \equiv \frac{N_R}{N_L + N_R} = \frac{n_R}{\sigma_L + \sigma_R} \tag{2.6}$$

by using of which one can express n_L and n_R as follows:

$$n_L = (1 - p)(\sigma_L + \sigma_R), \tag{2.7}$$

$$n_R = p(\sigma_L + \sigma_R). \tag{2.8}$$

If the local electroneutrality holds on both plates, i.e., $n_L = \sigma_L$ and $n_R = \sigma_R$, then the order parameter p equals to

$$p_{\text{neutr}} = \frac{A}{1 + A}. \tag{2.9}$$

(1) For the symmetric case $A = 1$ with $\sigma_L = \sigma_R = \sigma$, upon changing the distance between plates from 0 to ∞, a sequence of five phases I–V emerges [42–47]. These staggered phases consist of two equivalent lattice structures on the left and right plates, shifted with respect to one another by a half period in both spatial directions. Phase I, the monolayer hexagonal structure, exists only at zero interplate distance $d = 0$ [44,47]. Phase II corresponds to a staggered rectangular bilayer with the aspect ratio $1 < \Delta < \sqrt{3}$, phase III is a staggered square bilayer, phase IV a staggered rhombic bilayer with a deformation angle $\varphi < \pi/2$, and phase V a staggered hexagonal bilayer. Since $N_L = N_R = N/2$ for each of the phases, it holds that $n_L = n_R = \sigma$ or, equivalently, $p_{\text{gs}} = \frac{1}{2}$ where the subscript "gs" means "ground state." Each plate as a whole (i.e., the surface charge density plus the counterions) is thus neutral. As a consequence, the walls are bounded at large distances by short-ranged (usually exponentially decaying) forces.

(2) The asymmetric case $0 < A < 1$, studied by using both analytical calculations and computational evolutionary techniques as well as unsupervised learning in Refs. [48–50], exhibits much more phases. In an interval of small distances up to a critical one, $0 \leqslant d < d_c(A)$, phase I with all counterions collapsed onto the hexagonal monolayer on the left plate is dominant, i.e.,

$$n_L = \sigma_L + \sigma_R, \quad n_R = 0. \tag{2.10}$$

Consequently,

$$p_{\text{gs}}(d) = 0 \quad \text{for } 0 \leqslant d \leqslant d_c(A). \tag{2.11}$$

In the opposite asymptotic limit of large distances $d \to \infty$, the local neutralization of each of the plates by the corresponding counterions takes place:

$$\lim_{d\to\infty} n_L(d) = \sigma_L, \quad \lim_{d\to\infty} n_R(d) = \sigma_R. \tag{2.12}$$

Consequently,

$$\lim_{d\to\infty} p_{\text{gs}}(d) = p_{\text{neutr}}. \tag{2.13}$$

As a rule, $p_{\text{gs}}(d)$ grows from 0 to p_{neutr} monotonously with increasing distance d. In general, for finite interplate distances d, the counterion densities $n_L \neq \sigma_L$ and $n_R \neq \sigma_R$ do not neutralize locally the corresponding surface charge densities at the plates. This implies long-ranged (inverse-power law) effective interactions between the plates at large distances [48,49].

C. Nonzero temperatures, $T > 0$

As soon as $T > 0$, the counterions can move into the slab interior. When the temperature is low, the counterions are still localized in the neighborhood of the plate they belonged at zero temperature and one can adopt plausibly the counterparts of the densities n_L and n_R; they do not represent the counterion densities *at* the walls but rather *under the effect of the effective fields* generated by the corresponding walls.

(1) For the symmetrically charged plates, the reflection symmetry of the system keeps the local electroneutrality of the plates, $n_L = n_R = \sigma$, and so, likewise in the ground state, $p = \frac{1}{2}$. This is behind the success of the method of interest [40] to describe the thermodynamics for nonzero temperatures in terms of ground-state effective fields.

(2) For asymmetrically charged plates, in close analogy with the zero temperature, the counterion densities are not expected to neutralize locally the corresponding surface charge densities at the plates for finite distances, i.e., in general,

$n_L \neq \sigma_L$ and $n_R \neq \sigma_R$. A crucial complication for asymmetric plates is a discontinuous change of counterion densities n_L and n_R when passing from zero to nonzero temperatures. As will be shown later both analytically as well as numerically, the counterion densities skip from values $n_L = (\sigma_L + \sigma_R)$ and $n_R = 0$ to $n_L = n_R = (\sigma_L + \sigma_R)/2$ at asymptotically small distances, as soon as T goes from 0 to a nonzero value. This is because for small interplate distances the counterions move freely in the electric field created by the uniformly charged plates (the potential difference between the plates is very small) and the neighboring counterions are sufficiently far away from each other for having any effect on the electric field in the direction perpendicular to the plates. Consequently,

$$p(d) \sim \tfrac{1}{2} \quad \text{for } d \to 0^+. \tag{2.14}$$

We conclude that for small distances going from $T = 0$ to $T > 0$ induces a discontinuity in p from $p_{\rm gs} = 0$ (2.11) to $p = \frac{1}{2}$ (2.14), respectively. To extend the ground-state description in terms of effective fields to nonzero temperatures is then nontrivial due to atypical entropy contributions.

III. GROUND-STATE PICTURE

To neutralize the plate surface with a fixed surface charge density $e\sigma$ by a regular lattice structure of point charges $-e$, the lattice constant should be of order $1/\sqrt{\sigma}$. At zero temperature, the distance between the plates will be considered in the dimensionless form

$$\eta = d\sqrt{\frac{\sigma_L + \sigma_R}{2}}. \tag{3.1}$$

Roughly speaking, the parameter η is the ratio of the distance between the plates d and the characteristic distance between the nearest-neighbor counterions on the plates.

There are two ways to obtain the ground-state pressure: either via the counterion density at the wall contact (contact theorem, see below), or the energy change with the interplate distance.

A. Contact pressure

Under the term "effective field" we understand the factor by which the electric field created by the fixed surface charge density of a plate is screened by counterion layers. Let us derive first, in Gaussian units, the effective field acting on counterions constrained to the left plate. The electric field generated by the uniform surface charge density $e\sigma_L$ is given by

$$E_L = 2\pi e\sigma_L. \tag{3.2}$$

For a single counterion on the left plate ($z = 0$), the layer of counterions on the same plate induces a symmetric potential $V(z) = V(-z)$ and therefore the electric field $E = -\partial V(z)/\partial z$, proportional to z, is subdominant with respect to Eq. (3.2). The discrete layer of ions on the opposite right plate, together with the uniform surface charge density $e\sigma_R$ on that plate, renormalize the bare field E_L by a factor κ_L which depends on the distance η. For small distances $\eta \to 0$, each counterions on the left plate feels the electric field generated by the two plates only $2\pi e(\sigma_L - \sigma_R)$, while discrete layers of other counterions are too far away compared to the interplate distance to contribute to the energy, i.e., $\kappa_L = (\sigma_L - \sigma_R)/\sigma_L$. For large distances $\eta \to \infty$, the discrete character of the counterion layer on the opposite right plate becomes irrelevant and together with the fixed surface charge density they form a neutral entity, i.e., $\kappa_L = 1$. To summarize,

$$\kappa_L \underset{\eta\to 0}{\sim} 1 - A, \quad \kappa_L \underset{\eta\to\infty}{\sim} 1. \tag{3.3}$$

Note that these limiting values of the effective field are not restricted to the ground state, but they apply also to nonzero temperatures.

Each ion at the contact with the left plate pushes on it with a force $\kappa_L eE_L$; since there are n_L ions per unit surface, the repulsive force per unit surface is $\kappa_L en_L E_L$. However, there is an electrostatic force acting on the left plate due to the presence of two (left and right) ion layers and of the surface charge on the right plate. Since the corresponding surface charge density $-e\sigma_L$ is opposite to the original one on the left plate, the attractive force per unit surface is $-2\pi(e\sigma_L)^2 = -e\sigma_L E_L$. The total force per unit surface, i.e., the pressure, is the sum of the contact and electrostatic forces:

$$\begin{aligned} P_0 &= \kappa_L en_L E_L - e\sigma_L E_L \\ &= 2\pi e^2\left(\kappa_L\sigma_L n_L - \sigma_L^2\right). \end{aligned} \tag{3.4}$$

In this paper, we follow the convention of Refs. [37,52] that all thermodynamic quantities will be rescaled to their dimensionless forms with respect to the *left* plate. In particular, the pressure will be considered in the dimensionless form

$$\widetilde{P}_0 \equiv \frac{P_0}{2\pi e^2\sigma_L^2}. \tag{3.5}$$

Thus, the dimensionless form of the relation (3.4) reads as

$$\widetilde{P}_0 = \frac{\kappa_L n_L}{\sigma_L} - 1. \tag{3.6}$$

An analogous analysis for the counterions on the right plate implies that

$$\widetilde{P}_0 = A^2\left(\frac{\kappa_R n_R}{\sigma_R} - 1\right). \tag{3.7}$$

Here, the factor κ_R renormalizes the bare field induced by the right plate $E_R = -2\pi e\sigma_R$ due to the presence of the homogeneous surface charge density and the discrete layer of ions on the opposite left plate. The counterparts of the limiting values (3.3) read as

$$\kappa_R \underset{\eta\to 0}{\sim} 1 - \frac{1}{A}, \quad \kappa_R \underset{\eta\to\infty}{\sim} 1. \tag{3.8}$$

The two equivalent relations for the pressure (3.6) and (3.7) imply the equality

$$\kappa_L n_L\sigma_L - \kappa_R n_R\sigma_R = \sigma_L^2 - \sigma_R^2 \tag{3.9}$$

or, equivalently,

$$\kappa_L(1 - p) - \kappa_R Ap = 1 - A. \tag{3.10}$$

B. Pressure obtained via the thermodynamic route

Definitions (3.6) and (3.7) of the dimensionless pressure were given in terms of the quantities at the plate contacts. Let

us introduce the auxiliary quantity $E_0(\eta, p)$ as the ground-state energy per unit surface in the subspace with a fixed order parameter p. One can define the pressure alternatively as (minus) the total derivative of this energy with respect to the distance:

$$P_0(\eta, p) = -\frac{d}{dd}\frac{E_0(\eta, p)}{S} = -\frac{e^2}{\sqrt{2}}(\sigma_L + \sigma_R)^2 \frac{d}{d\eta}\frac{E_0(\eta, p)}{Ne^2\sqrt{\sigma_L + \sigma_R}}; \quad (3.11)$$

hereinafter, if not necessary, the explicit dependence of quantities on the asymmetry parameter A will not be indicated. The ground-state value of p is determined by the condition of the energy minimum:

$$\left.\frac{\partial E_0(\eta, p)}{\partial p}\right|_{p=p_{\rm gs}} = 0, \quad \left.\frac{\partial^2 E_0(\eta, p)}{\partial p^2}\right|_{p=p_{\rm gs}} < 0. \quad (3.12)$$

The dimensionless pressure (3.5) is thus expressible as

$$\widetilde{P}_0(\eta, p) = -\frac{1}{2^{3/2}\pi}(1+A)^2 \frac{\partial}{\partial\eta}\frac{E_0(\eta, p)}{Ne^2\sqrt{\sigma_L + \sigma_R}}, \quad (3.13)$$

where the interchange of the total derivative by the partial one is possible due to the stationarity condition (3.12). In the ground state, the physical values of all considered quantities is taken at $p = p_{\rm gs}$, in particular,

$$\widetilde{P}_{\rm gs}(\eta) = \widetilde{P}_0(\eta, p_{\rm gs}). \quad (3.14)$$

From Eq. (3.6) one can express the combination

$$\frac{\kappa_L n_L}{\sigma_L} = 1 + \widetilde{P}_0(\eta, p). \quad (3.15)$$

With regard to Eq. (2.7), it holds that

$$\kappa_L(\eta, p) = \frac{1}{(1-p)(1+A)}[1 + \widetilde{P}_0(\eta, p)] = 1 - A + ApK_0(\eta, p), \quad (3.16)$$

where the function $K_0(\eta, p)$ is defined by

$$K_0(\eta, p) = \frac{\widetilde{P}_0(\eta, p) + A^2 + p(1-A^2)}{p(1-p)A(1+A)}. \quad (3.17)$$

Similarly, it follows from Eq. (3.7) that

$$\frac{\kappa_R n_R}{\sigma_R} = 1 + \frac{1}{A^2}\widetilde{P}_0(\eta, p). \quad (3.18)$$

Since $n_R = p(\sigma_L + \sigma_R)$, one ends up with

$$\kappa_R(\eta, p) = \frac{1}{p(1+A)}\left[A + \frac{1}{A}\widetilde{P}_0(\eta, p)\right] = 1 - \frac{1}{A} + (1-p)K_0(\eta, p). \quad (3.19)$$

The ground-state values of the effective fields are given by

$$\kappa_L^{\rm (gs)}(\eta) = \kappa_L(\eta, p_{\rm gs}), \quad \kappa_R^{\rm (gs)}(\eta) = \kappa_R(\eta, p_{\rm gs}). \quad (3.20)$$

C. Ground-state structures

The above discussion was quite general, valid for any type of the bilayer. In what follows, we shall restrict ourselves to the description of the relevant phases present in the phase diagram at small and large values of the distance η. The exotic (snub square, pentagonal,...) phases, taking place at intermediate interplate distances, are irrelevant for our purposes.

According to the general analysis presented in Appendix A of Ref. [49], the total energy $E(\eta, p, A)$ of any bilayer system with nonneutral (surface charge plus counterions) plates can be expressed in terms of the total energy of the bilayer system with "neutralized" plates, keeping the same values of η, p and fixing the neutral value of the asymmetry parameter $A = p/(1-p)$, as follows:

$$\frac{E_0(\eta, p; A)}{Ne^2\sqrt{\sigma_L + \sigma_R}} = \frac{E_0^{\rm neutr}(\eta, p; A = p/(1-p))}{Ne^2\sqrt{\sigma_L + \sigma_R}} + 2^{3/2}\pi\eta\left(p - \frac{A}{1+A}\right)^2. \quad (3.21)$$

The second term on the right-hand side of this equation is simply the excess energy due to the nonneutrality of each of the two plate's entities.

1. *Structures I and I_p emerging at small η*

As was mentioned in the Introduction, at small distances $\eta \in [0, \eta_c(A)]$, all counterions collapse onto the left plate in the so-called phase I [48,49], see the relations (2.10) implying that $p_{\rm gs} = 0$. Here, $\eta_c(A)$ is a critical distance at which a second-order transition from phase I to another one with $p_{\rm gs} > 0$ and a smaller energy takes place. The value of $\eta_c(A)$ increases with decreasing A; it goes from $\eta_c = 0$ for the symmetrically charged $A = 1$ plates up to $\eta_c \to \infty$ when $A = 0$ ($\sigma_R = 0$). The lattice spacing a of the hexagonal structure of counterions at the left plate is determined by the relation $\sqrt{3}a^2(\sigma_L + \sigma_R)/2 = 1$. The energy of phase I, $E_{\rm I}(\eta, A)$, is given by [48,49]

$$\frac{E_{\rm I}(\eta, A)}{Ne^2\sqrt{\sigma_L + \sigma_R}} = c + 2^{3/2}\pi\eta\left(\frac{A}{1+A}\right)^2, \quad (3.22)$$

with

$$c = \frac{1}{2^{3/2}\sqrt{\pi}}\int_0^\infty \frac{dt}{\sqrt{t}}\left\{\left[\theta_3(e^{-\sqrt{3}t})\theta_3(e^{-t/\sqrt{3}}) - 1 - \frac{\pi}{t}\right] + \left[\theta_2(e^{-\sqrt{3}t})\theta_2(e^{-t/\sqrt{3}}) - \frac{\pi}{t}\right]\right\} = -1.960515789\ldots, \quad (3.23)$$

being the Madelung constant of the 2D hexagonal structure; here, $\theta_2(q) = \sum_{j=-\infty}^{\infty} q^{(j-\frac{1}{2})^2}$ and $\theta_3(q) = \sum_{j=-\infty}^{\infty} q^{j^2}$ are Jacobi theta functions with zero argument. According to Eq. (3.13), the dimensionless pressure

$$\widetilde{P}_{\rm gs}(\eta) = -A^2 \quad (3.24)$$

is constant in phase I. The same result follows directly by inserting $n_R = 0$ into the formula (3.7) which confirms the consistency of the ground-state formalism.

When η exceeds its critical value $\eta_c(A)$, some of the counterions on the left plate start to jump perpendicularly to the right plate, i.e., the projections of the counterions of both layers onto one plane still form the hexagonal lattice. The corresponding phase with the given value of p is referred to as phase $\rm I_p$. There are specific "commensurate" values of

$p \in \{\frac{1}{2}, \frac{1}{3}, \frac{1}{4}, \frac{1}{7}, \frac{1}{9}, ...\}$ for which the counterions on the right place form an energetically favorable hexagonal lattice with spacing $b \geqslant a$. The interaction Coulomb energy of phase I_p is presented in Appendix A. Since the distribution of commensurate values of p becomes denser and denser as $p \to 0$, it is natural to extend the formulas for the energy (A1) and (A2) to continuous values of p in this limit of $p \to 0$.

In the region of small p, the expression for the energy (A1) can be expanded systematically in powers of p [49]:

$$\frac{E_{\mathrm{I}_p}(\eta, p) - E_{\mathrm{I}}(\eta, p)}{Ne^2\sqrt{\sigma_L + \sigma_R}} = f(\eta)p + \frac{2^{3/2}\pi}{\lambda}\eta^2 p^{5/2} + \mathcal{O}(p^{7/2}), \tag{3.25}$$

where

$$f(\eta) = 2^{3/2}\pi\frac{1-A}{1+A}\eta - \frac{1}{\sqrt{2\pi}}\int_0^\infty \frac{dt}{\sqrt{t}}\left(1 - e^{-\eta^2 t}\right) \times [\theta_3(e^{-\sqrt{3}t})\theta_3(e^{-t/\sqrt{3}}) - 1 + \theta_2(e^{-\sqrt{3}t})\theta_2(e^{-t/\sqrt{3}})] \tag{3.26}$$

and

$$\lambda = \frac{4\pi}{3^{1/4}\zeta\left(\frac{3}{2}\right)\left[\zeta\left(\frac{3}{2}, \frac{1}{3}\right) - \zeta\left(\frac{3}{2}, \frac{2}{3}\right)\right]} \simeq 0.999215. \tag{3.27}$$

Here, $\zeta(s, q) = \sum_{j=0}^\infty 1/(q+j)^s$ is the Hurwitz ζ function which represents the generalization of the Riemann ζ function $\zeta(s) \equiv \zeta(s, 1)$. The extremum condition for the energy of phase I_p (3.25) reads as

$$0 = f(\eta) + \frac{5\sqrt{2}\pi}{\lambda}\eta^2 p^{3/2} + \mathcal{O}(p^{5/2}). \tag{3.28}$$

For a given A, the critical value of the dimensionless distance is identified with the condition $f(\eta_c) = 0$, i.e.,

$$4\pi\frac{1-A}{1+A}\eta_c = \frac{1}{\sqrt{\pi}}\int_0^\infty \frac{dt}{\sqrt{t}}(1 - e^{-\eta_c^2 t}) \times [\theta_3(e^{-\sqrt{3}t})\theta_3(e^{-t/\sqrt{3}}) - 1 + \theta_2(e^{-\sqrt{3}t})\theta_2(e^{-t/\sqrt{3}})]. \tag{3.29}$$

The function $f(\eta)$ (3.26) is dominated by the positive linear term for small η, so that $f(\eta) > 0$ for $0 \leqslant \eta < \eta_c$ and $f(\eta) < 0$ for $\eta > \eta_c$. In the region $0 \leqslant \eta < \eta_c$, in the vicinity of the critical point, $f(\eta)$ can be expanded as $f(\eta) \sim g(\eta_c - \eta)$ with a positive prefactor $g > 0$. In the region $0 < \eta < \eta_c$, the extremum equation (3.28) has no real solution for p; the minimum energy is determined by $p = 0$ (phase I) in that region. However, the extremum equation (3.28) has a positive (real) solution for p in the region $\eta > \eta_c$, $p(\eta) \propto (\eta - \eta_c)^{2/3}$, which grows continuously from 0 at $\eta = \eta_c$. It is simple to verify that this solution provides the minimum of the energy within the phase I_p.

2. *Structure* V_p *emerging at large* η

The energy of phase V_p is presented in Eq. (B1). The large-η asymptotic of the integral (B2) was calculated by using the saddle-point method in Appendix E of Ref. [49], with the result

$$J(\eta, p) \underset{\eta\to\infty}{\sim} -\frac{3^{5/4}}{\sqrt{2}}p\sqrt{1-p}\exp\left(-\frac{4\pi\sqrt{1-p}}{3^{1/4}}\eta\right). \tag{3.30}$$

This integral decays exponentially in η and therefore it can be neglected comparing the term of the order η in Eq. (B1), i.e.,

$$\frac{E_{\mathrm{V}_p}(\eta, p)}{Ne^2\sqrt{\sigma_L + \sigma_R}} \underset{\eta\to\infty}{\sim} 2^{3/2}\pi\eta\left(p - \frac{A}{1+A}\right)^2 + c[(1-p)^{3/2} + p^{3/2}]. \tag{3.31}$$

According to Eq. (3.13), the dimensionless pressure behaves as

$$\widetilde{P}_0(\eta, p) = -(1+A)^2\left(p - \frac{A}{1+A}\right)^2 \tag{3.32}$$

and the function $K_0(\eta, p)$ (3.17) is constant:

$$K_0(\eta, p) = \frac{1+A}{A}. \tag{3.33}$$

The effective fields

$$\kappa_L(\eta, p) = 1 - A + p(1+A), \tag{3.34}$$

$$\kappa_R(\eta, p) = 2 - p\left(\frac{1+A}{A}\right) \tag{3.35}$$

depend only on the order parameter p.

For fixed values of the parameters (η, A), the ground-state value of p is determined by the condition of the energy minimum (3.12) as follows:

$$2^{5/2}\pi\eta\left(p_{\mathrm{gs}} - \frac{A}{1+A}\right) + \frac{3}{2}c(\sqrt{p_{\mathrm{gs}}} - \sqrt{1-p_{\mathrm{gs}}}) = 0. \tag{3.36}$$

Consequently, at large η,

$$p_{\mathrm{gs}} \underset{\eta\to\infty}{\sim} p_{\mathrm{neutr}} - \frac{3(-c)}{2^{7/2}\pi}\frac{1-\sqrt{A}}{\sqrt{1+A}}\frac{1}{\eta}. \tag{3.37}$$

Since c is negative, p_{gs} tends to its asymptotic value $p_{\mathrm{neutr}} = A/(1+A)$ from below; this means that the number of counterions on the right plate $N_R < \sigma_R S$ and the number of counterions on the left plate $N_L > \sigma_L S$. The ground-state energy of phase V_p has the large-η asymptotic

$$\frac{E_{\mathrm{gs}}(\eta)}{Ne^2\sqrt{\sigma_L + \sigma_R}} \underset{\eta\to\infty}{\sim} c\frac{1+A^{3/2}}{(1+A)^{3/2}} - \frac{9c^2}{2^{11/2}\pi}\frac{(1-\sqrt{A})^2}{1+A}\frac{1}{\eta}. \tag{3.38}$$

Inserting into Eq. (3.32) $p = p_{\mathrm{gs}}$ from Eq. (3.37), the ground-state pressure exhibits the following asymptotic behavior

$$\widetilde{P}_{\mathrm{gs}}(\eta) \underset{\eta\to\infty}{\sim} -\frac{9c^2}{2^7\pi^2}(1-\sqrt{A})^2(1+A)\frac{1}{\eta^2}. \tag{3.39}$$

This formula is nonuniversal because it contains the Madelung constant c of the hexagonal Wigner structure and the asymmetry parameter A. As $\widetilde{P}_{\mathrm{gs}}$ goes at asymptotically large distances to 0 from below, the asymmetric plates attract one another.

In the symmetric case $A = 1$, the leading long-range $1/\eta^2$ term in Eq. (3.39) vanishes and the standard short-range exponential attraction [47]

$$\widetilde{P}_{\mathrm{gs}}(\eta) \underset{\eta\to\infty}{\sim} -3\exp\left(-\frac{4\pi\eta}{\sqrt{2}3^{1/4}}\right) \tag{3.40}$$

takes place. This results does not contradict the previous formula since exponentially decaying contributions were neglected in the derivation of Eq. (3.39).

IV. NONZERO TEMPERATURES

The system is considered to be in thermal equilibrium at the inverse temperature $\beta = 1/(k_{\rm B}T)$. Besides the dimensionless distance η (3.1) introduced in the ground state, there are two other length scales relevant for nonzero temperatures. The Bjerrum length $\ell_{\rm B}$ is the distance at which two unit charges interact with the thermal energy $k_{\rm B}T$, $\ell_{\rm B} = \beta e^2$. Respecting our convention, the Gouy-Chapman length μ is the distance from the left plate at which the potential energy induced by the surface charge density $e\sigma_L$ equals to the thermal energy $k_{\rm B}T$,

$$\mu = \frac{1}{2\pi \ell_{\rm B}\sigma_L}. \tag{4.1}$$

The perpendicular z coordinate will be expressed in units of μ:

$$\widetilde{z} \equiv \frac{z}{\mu}. \tag{4.2}$$

The dimensionless coupling parameter Ξ, reflecting the strength of electrostatic correlations, is defined as the ratio of the two length scales,

$$\Xi \equiv \frac{\ell_{\rm B}}{\mu} = 2\pi \ell_{\rm B}^2 \sigma_L. \tag{4.3}$$

The dimensionless distance η (3.1) is expressible in terms of $\widetilde{d} = d/\mu$ as follows:

$$\eta = \sqrt{1+A}\frac{\widetilde{d}}{2\sqrt{\pi\,\Xi}}. \tag{4.4}$$

As in the ground state, the pressure can be obtained via either the contact theorem or the thermodynamic route.

A. Contact pressure

At nonzero yet not too large temperatures, the smear of the (left or right) ionic layer due to thermal noise is much smaller than the interion spacing within the given layer. One can thus adopt the single-particle ground-state picture with the precisely same effective fields acting on counterions close to the left and right plates. There is an effective electric field $\kappa_L E_L$ [with E_L given by Eq. (3.2)] acting on counterions attached to the left plate, the corresponding potential reads as $V_L(z) = -\kappa_L E_L z$. Thermal equilibrium at nonzero temperature is turned on via the position-dependent counterion density in space $n_L(z)$ which is proportional to the one-body Boltzmann factor $\exp[-\beta(-e)V_L(z)]$:

$$n_L(z) = C_L \exp\left(-\kappa_L \widetilde{z}\right). \tag{4.5}$$

The 2D surface density of counterions n_L (which has dimension $1/(\text{length})^2$) is given as the integral along the perpendicular z axis of the density of counterions in 3D space $n_L(z)$ [which has dimension $1/(\text{length})^3$]:

$$n_L = \int_0^d dz\, n_L(z). \tag{4.6}$$

This normalization condition determines the prefactor C_L as follows:

$$C_L = \frac{\kappa_L n_L}{\mu}\frac{1}{1-e^{-\kappa_L \widetilde{d}}}. \tag{4.7}$$

Analogously, the spatial density of counterions attached to the right plate reads as

$$n_R(z) = C_R \exp[-\kappa_R A(\widetilde{d} - \widetilde{z})], \tag{4.8}$$

where the prefactor C_R is determined by the normalization condition $n_R = \int_0^d dz\, n_R(z)$ as follows:

$$C_R = \frac{\kappa_R n_R A}{\mu}\frac{1}{1-e^{-\kappa_R A\widetilde{d}}}. \tag{4.9}$$

The total density of counterions in space $n(z)$ is the sum of the left and right counterion densities:

$$n(z) = n_L(z) + n_R(z). \tag{4.10}$$

The order parameter p, introduced in the analytic treatment of asymmetric plates, cannot be deduced from numerical simulations at nonzero temperatures because it is not clear from the actual position of a counterion which is its plate of origin at zero temperature. However, the knowledge of the density profile in simulations motivates us to employ the half-space occupation quantity τ as the ratio of the number of counterions to the right of the midplane between the plates, $N^>$, to the total counterion number N,

$$\tau = \frac{N^>}{N}. \tag{4.11}$$

This quantity has already been introduced in Ref. [53] under the name "the total diffuse charge near the cathode." Since $N^> = N_L^> + N_R^>$, where

$$N_L^> = S\int_{d/2}^{d} dz\, n_L(z) = SC_L\mu \int_{\tilde{d}/2}^{\tilde{d}} dz\, e^{-\kappa_L \tilde{z}} \tag{4.12}$$

and

$$N_R^> = S\int_{d/2}^{d} dz\, n_R(z) = SC_R\mu \int_{\tilde{d}/2}^{\tilde{d}} dz\, e^{-\kappa_R A(\tilde{d}-\tilde{z})}, \tag{4.13}$$

the theoretically predicted value of τ takes the explicit form

$$\tau(\eta, p) = (1-p)\frac{1}{e^{\kappa_L \tilde{d}/2}+1} + p\frac{1}{e^{-\kappa_R A\tilde{d}/2}+1}. \tag{4.14}$$

The limiting $\eta \to 0$ and $\eta \to \infty$ values of τ coincide with those of p:

$$\lim_{\eta\to 0}\tau = \frac{1}{2}, \quad \lim_{\eta\to\infty}\tau = \frac{A}{1+A}. \tag{4.15}$$

Having the density profile of counterions, the pressure P_c can be obtained by applying the contact value theorem for planar wall surfaces [54–57]. With respect to the left plate, the pressure is given by

$$\begin{aligned}\beta P_c &= n(0) - 2\pi \ell_{\rm B}\sigma_L^2 \\ &= C_L + C_R \exp(-\kappa_R A\widetilde{d}) - 2\pi \ell_{\rm B}\sigma_L^2.\end{aligned} \tag{4.16}$$

Introducing the dimensionless pressure

$$\widetilde{P}_c \equiv \frac{\beta P_c}{2\pi \ell_{\rm B}\sigma_L^2}, \tag{4.17}$$

one gets that

$$\widetilde{P}_c = \frac{\kappa_L n_L}{\sigma_L}\frac{1}{1-e^{-\kappa_L\widetilde{d}}} + \frac{\kappa_R n_R}{\sigma_R}A^2\frac{1}{e^{\kappa_R A\widetilde{d}}-1} - 1. \tag{4.18}$$

With respect to the right plate, the pressure is given by

$$\begin{aligned}\beta P_c &= n(d) - 2\pi\ell_{\rm B}\sigma_R^2 \\ &= C_L\exp(-\kappa_L\widetilde{d}) + C_R - 2\pi\ell_{\rm B}\sigma_R^2,\end{aligned} \tag{4.19}$$

so that

$$\widetilde{P}_c = \frac{\kappa_L n_L}{\sigma_L}\frac{1}{e^{\kappa_L\widetilde{d}}-1} + \frac{\kappa_R n_R}{\sigma_R}A^2\frac{1}{1-e^{-\kappa_R A\widetilde{d}}} - A^2. \tag{4.20}$$

The requirement of the equivalence of the two pressure representations (4.18) and (4.20),

$$\kappa_L(1-p) - \kappa_R A p = 1 - A, \tag{4.21}$$

coincides with the ground-state constraint for the left and right effective fields (3.10).

In analogy with the ground-state Eqs. (3.16) and (3.19), this constraint is fulfilled by the ansatz

$$\kappa_L(\eta, p) = 1 - A + ApK(\eta, p), \tag{4.22}$$

$$\kappa_R(\eta, x) = 1 - \frac{1}{A} + (1-p)K(\eta, p), \tag{4.23}$$

with $K(\eta, x)$ being an arbitrary function. The basic idea of the theory in Ref. [40] dealing with the symmetric case was that extending the ground-state effective fields to nonzero temperatures is a plausible approximation. The same idea is adopted to our asymmetric case by setting

$$K(\eta, p) = K_0(\eta, p), \tag{4.24}$$

with $K_0(\eta, p)$ defined by Eq. (3.17), in relations (4.22) and (4.23). In this way one obtains the ground-state representations (3.16) and (3.19).

Using formulas (4.18) and (4.20) for the effective fields, the pressure can be expressed in a symmetrized form:

$$\begin{aligned}\widetilde{P}_c = \frac{1}{2}\left[\frac{\kappa_L n_L}{\sigma_L}\coth\left(\frac{\kappa_L\widetilde{d}}{2}\right) + \frac{\kappa_R n_R}{\sigma_R}A^2\coth\left(\frac{\kappa_R A\widetilde{d}}{2}\right)\right] \\ - \frac{1+A^2}{2}.\end{aligned} \tag{4.25}$$

Applying here the expansion formula

$$\coth t = \frac{1}{t} + \frac{t}{3} + \mathcal{O}(t^3), \tag{4.26}$$

the limiting $\eta \to 0$ values of κ_L (3.3) and κ_R (3.8) and the constraint (3.9), the small-distance expansion of the pressure is expressible explicitly up to the first order in $\widetilde{d}$:

$$\widetilde{P}_c = \frac{1+A}{\widetilde{d}} - \frac{1+A^2}{2} + (1-A)^2(1+A)\frac{\widetilde{d}}{12} + \mathcal{O}(\widetilde{d}^2). \tag{4.27}$$

B. Pressure obtained via the thermodynamic route

In the canonical ensemble, having N_L counterions attached to the left plate and N_R counterions attached to the right plane, the free energy $F(N_L, N_R)$ is defined as

$$-\beta F(N_L, N_R) = \ln Z(N_L, N_R), \tag{4.28}$$

where $Z(N_L, N_R)$ is the partition function

$$\begin{aligned}Z_N = \frac{1}{(N_L+N_R)!}\int_\Lambda \prod_{j=1}^{N_L}\frac{d\mathbf{r}_j}{\lambda^3}\prod_{k=1}^{N_R}\frac{d\mathbf{r}_k}{\lambda^3} \\ \times \exp[-\beta E(\eta, x; \{\mathbf{r}_j\}, \{\mathbf{r}_k\})],\end{aligned} \tag{4.29}$$

where λ stands for the thermal de Broglie wavelength and $\Lambda = \{\mathbf{r}, 0 < z < d\}$ denotes the slab between the plates.

The total energy of counterions $E(\eta, x; \{\mathbf{r}_j\}, \{\mathbf{r}_k\})$ can be expanded around the ground-state energy in small deviations from their ground-state positions, as is done for symmetrically charged plates in Ref. [37],

$$\begin{aligned}\beta E(\{\mathbf{r}_j\}, \{\mathbf{r}_k\}) = \beta E_{\rm gs} + \kappa_L\sum_{j=1}^{N_L}\tilde{z}_j + \frac{\ell_{\rm B}}{2a_L^3}\sum_{j=1}^{N_L}\left(x_j^2+y_j^2\right) \\ + \kappa_R A\sum_{k=1}^{N_R}(\tilde{d}-\tilde{z}_k) + \frac{\ell_{\rm B}}{2a_R^3}\sum_{k=1}^{N_R}\left(x_k^2+y_k^2\right) \\ + \cdots.\end{aligned} \tag{4.30}$$

Here, $a_L \propto 1/\sqrt{n_L}$ and $a_R \propto 1/\sqrt{n_R}$ are the lattice spacings of counterion structures created on the left and right plates, respectively; the prefactors, which depend only on the particular lattice structures, are irrelevant for our purposes. Higher-order terms in Eq. (4.30) scale like $1/\Xi^{(a-2)/4}$ $(a = 3, 4\ldots)$ and therefore vanish in the limit $\Xi \to \infty$.

The integration of the Boltzmann factor with the energy (4.30) can be performed straightforwardly in Eq. (4.29) for the perpendicular z components:

$$\int_0^d \frac{dz_j}{\lambda}e^{-\kappa_L\tilde{z}_j} = \frac{\mu}{\lambda}\frac{1-e^{-\kappa_L\tilde{d}}}{\kappa_L}, \quad j = 1, \ldots, N_L \tag{4.31}$$

and

$$\int_0^d \frac{dz_k}{\lambda}e^{-\kappa_R A(\tilde{d}-\tilde{z}_k)} = \frac{\mu}{\lambda}\frac{1-e^{-\kappa_R A\tilde{d}}}{\kappa_R A}, \quad k = 1, \ldots, N_R. \tag{4.32}$$

The parallel components x, y are trickier. Let us assume first that due to strong electrostatic repulsions in the parallel (x, y) plane a given counterion (say the one sitting on the left plate) is constrained to the space $S/N_L = 1/n_L$ reserved for one counterion, namely to a disk of radius R_L given by $R_L^2 = 1/(\pi n_L)$. In radial coordinates, the integration over coordinates x, y reads as

$$\int_0^{R_L} 2\pi r dr\exp\left(-\frac{\ell_{\rm B}}{2a_L^3}r^2\right) = \frac{2\pi a_L^3}{\ell_{\rm B}}\int_0^{\frac{\ell_{\rm B}}{2\pi n_L a_L^3}} dt\, e^{-t}. \tag{4.33}$$

Since the upper limit of integration

$$\frac{\ell_{\rm B}}{2\pi n_L a_L^3} \propto \frac{\ell_{\rm B}}{a_L} \propto \sqrt{\Xi}\sqrt{\frac{n_L}{\sigma_L}}, \tag{4.34}$$

the integral over t in Eq. (4.33) equals to 1 in the large-Ξ limit. Consequently, the integration over coordinates x, y implies for every counterion the factor $\propto n_L^{-3/2}$ where the explicit form of the constant prefactor is irrelevant. Similarly, the corresponding factor for each counterion sitting on the right plate can be shown to be $\propto n_R^{-3/2}$.

To summarize the above paragraph, the free energy (4.28) can be expressed as

$$-\beta F(N_L,N_R) = \text{const} - \beta E_{\text{gs}} + N_L \ln\left(\frac{1-e^{-\kappa_L \tilde{d}}}{\kappa_L}\right) - \frac{3}{2}N_L \ln n_L + N_R \ln\left(\frac{1-e^{-\kappa_R A\tilde{d}}}{A\kappa_R}\right) - \frac{3}{2}N_R \ln n_R. \tag{4.35}$$

Thus, the free energy per counterion $f = F/(N_L+N_R)$ is given by

$$\beta f(\eta,p) = \text{const} + \frac{\beta E_{\text{gs}}(\eta,p)}{N} - (1-p)\ln\left(\frac{1-e^{-\kappa_L\tilde{d}}}{\kappa_L}\right) + \frac{3}{2}(1-p)\ln(1-p) - p\ln\left(\frac{1-e^{-\kappa_R A\tilde{d}}}{A\kappa_R}\right) + \frac{3}{2}p\ln p. \tag{4.36}$$

The thermodynamic pressure is defined as (minus) the total derivative of the free energy with respect to the distance:

$$P_{\text{th}}(\eta,p) = -\frac{d}{dd}\frac{F(\eta,p)}{S} = -\frac{1}{\sqrt{2}}(\sigma_L+\sigma_R)^{3/2}\frac{df(\eta,p)}{d\eta}. \tag{4.37}$$

The value of the order parameter p is determined by the variational condition of the free-energy minimum:

$$\frac{\partial f(\eta,x)}{\partial x} = 0, \quad \frac{\partial^2 f(\eta,x)}{\partial x^2} < 0. \tag{4.38}$$

The dimensionless thermodynamic pressure $\widetilde{P}_{\text{th}} \equiv \beta P_{\text{th}}/(2\pi\ell_{\text{B}}\sigma_L^2)$ is thus expressible as

$$\widetilde{P}_{\text{th}}(\eta,p) = -\frac{1}{2^{3/2}\pi}(1+A)^2\frac{\partial}{\partial\eta}\frac{\beta f(\eta,p)}{\ell_{\text{B}}\sqrt{\sigma_L+\sigma_R}}, \tag{4.39}$$

where the replacement of the total derivative by the partial one is possible due to the stationarity condition (4.38).

As soon as the temperature is nonzero, i.e., for any finite value of the coupling constant Ξ, the effective force (pressure) between two symmetrically charged walls at asymptotic (in fact, extremely large) distances between the walls $d \to \infty$ is expected to be *repulsive*, of the PB power-law type [30,35,58–60]

$$\beta P \underset{d\to\infty}{\sim} \frac{\pi}{2\ell_{\text{B}}}\frac{1}{d^2}, \quad \widetilde{P} \underset{\tilde{d}\to\infty}{\sim} \frac{\pi^2}{\tilde{d}^2}. \tag{4.40}$$

The validity of this asymptotic relation for asymmetric plates (but with the same sign of the charge) was shown in Ref. [52]. Note the universal independence of the repulsive pressure (4.40) on the surface charge densities of the plates, the only condition is that the plates bear surface charges of the same sign. For asymmetric plates, the scaling (4.40) is fulfilled at larger distances compared to symmetric plates.

As was shown in the previous section, at zero temperature phase V_p is relevant at asymptotically large distances, leading to an *attractive* pressure with the asymptotic nonuniversal behavior (3.39) which has the same $1/d^2$-dependence on the distance as the PB pressure (4.40). At low enough temperatures, the attractive regime still exists and spreads over a large interval of distances, except for asymptotically large distances where the PB repulsion takes place. One can intuitively expect the impact of phase V_x on the large-distance behavior of the attractive pressure within the given interval of distances. To be more particular, let us consider the ground-state energy (3.31) with the effective fields (3.34) and (3.35) in the expression for the free energy (4.36). The exponentially decaying terms of type $\exp(-\kappa_L\tilde{d})$ and $\exp(-\kappa_R A\tilde{d})$ are negligible comparing with their inverse-power-law counterparts, thus the free energy is given by

$$\frac{\beta f(\eta,p)}{\ell_{\text{B}}\sqrt{\sigma_L+\sigma_R}} = \text{const} + 2^{3/2}\pi\eta\left(p-\frac{A}{1+A}\right)^2 + c[(1-p)^{3/2}+p^{3/2}] + \sqrt{\frac{2\pi}{(1+A)\Xi}} \times \Big\{(1-p)\ln[1-A+p(1+A)] + \frac{3}{2}(1-p)\ln(1-p) + p\ln[2A-p(1+A)] + \frac{3}{2}p\ln p\Big\}. \tag{4.41}$$

The variational condition (4.38) implies that for large η

$$p \sim \frac{A}{1+A} + \frac{a}{\eta}, \quad a = \frac{3c}{2^{7/2}\pi}\frac{1-\sqrt{A}}{\sqrt{1+A}} - \frac{5}{8\sqrt{\pi\Xi}}\frac{\ln A}{\sqrt{1+A}}. \tag{4.42}$$

In the zero-temperature limit $\Xi \to \infty$, this formula reduces to the previous ground-state one (3.39) as it should be. The thermodynamic pressure (4.39) behaves for large η as follows:

$$\widetilde{P}_{\text{th}} = -(1+A)^2\left(p-\frac{A}{1+A}\right)^2 \sim -(1+A)^2\frac{a^2}{\eta^2}. \tag{4.43}$$

This scaling dependence on the distance between the plates, which holds exclusively in the large-distance region of the attractive pressure, has the functional form of the repulsive PB pressure (4.40), with a nonuniversal prefactor.

V. MONTE CARLO SIMULATIONS

Metropolis MC simulations were carried out in a quasi-2D slab geometry, where x and y directions are periodic. The last z direction is bound by two charged, planar, and hard surfaces, with uniform surface charge densities σ_L and σ_R. We used $N = 384$ mobile point charges, which neutralize the surface charges, and varied both the electrostatic coupling parameter Ξ and separation d between the two charged plates. The point charges were confined to the slab between the two surfaces. Electrostatic interactions were handled with standard Ewald summation techniques, where we introduced an extra vacuum slab between the periodic images in the z-direction, with corrections for the quasi-2D dimensionality and the extra vacuum slab [61,62]. The correction term in our case (keeping

only terms dependent on the mobile charges positions) equals

$$\beta U_{q2\mathrm{D}} = 2\pi l_B \left[\frac{1}{(d+v)S} \left(\sum_i q_i z_i \right)^2 + \frac{(\sigma_L + \sigma_R)}{(d+v)} \sum_i q_i z_i^2 + (\sigma_R - \sigma_L) \sum_i q_i z_i \right], \quad (5.1)$$

where v is the length of the vacuum slab, S the area of either of the surfaces, z_i the perpendicular position of the charges (where the midplane is defined as $z = 0$), and q_i the valency of charge i. The vacuum slab was usually set to be $v = 200\,\mu$ wide. Tests with larger slabs were performed but without any detectable difference. We also varied the precision of the Ewald summation, including more terms in the Fourier space summation and faster damping of the real part, but again, without any detectable differences compared to the reported data. New trial configurations were generated by randomly displacing them a certain distance, with an acceptance ratio close to around 30–50% using the Metropolis MC algorithm. For a tenth of these displacements, we also tried to mirror a point charge around the midplane to the other surface. All data points were pre-equilibrated for 10^4 MC cycles, where one cycles corresponds to N trial displacements. Pressures and ion density profiles were then collected over 10^5 MC cycles. Pressures were either calculated by estimating the contact value of the ion densities at the respective surface, minus either $2\pi\sigma_L^2$ or $2\pi\sigma_R^2$ accounting for the electrostatic interaction between the smeared-out charge of the surfaces with the rest of the system, or over the midplane. The latter involves both estimating the midplane concentration and all the electrostatic forces acting across the midplane [20]. While both estimates of the pressures are the same, the latter is usually more precise. Standard errors in pressure were estimated by applying block-averages, using ten blocks.

VI. COMPARISON OF THE THEORY WITH MONTE CARLO DATA

All MC simulations were done with the asymmetry parameter $A = \frac{1}{2}$. The thermodynamic quantities of interest are the (dimensionless) pressure $\widetilde{P}$ (4.17) and the half-space occupation parameter τ defined by Eq. (4.11).

For very large values of the coupling constant $\Xi > 300$, the results of the theory agree remarkably with MC data; to spare space we do not present them.

The results for the pressure $\widetilde{P}$ as the function of the distance $\tilde{d}$ for the intermediate value of the coupling constant $\Xi = 100$ are presented in Fig. 2. The MC data are represented by solid line and the results of the present theory by dashed line; the thermodynamic route to obtain the pressure provides more reliable results than the contact value theorem, so theoretical results are taken for that pressure. The results of the present theory are limited to the range of distances $0 < \tilde{d} \lesssim 25$, where the ground state corresponds to the phases I and I_x; for larger distances where the phase V_x prevails, see the large-distance analysis of the attracive pressure at the end of Sec. IV. It is seen that the agreement of the theory and MC simulations is excellent also for this not too-large value of Ξ. The leading term of the virial SC (VSC) theory for the asymmetrically

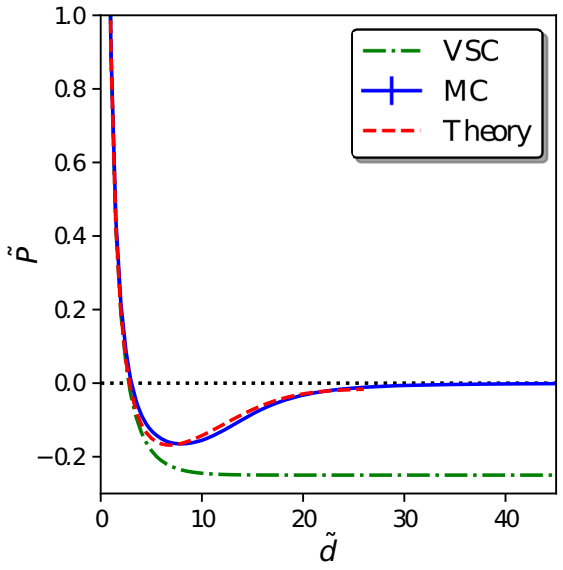

FIG. 2. The pressure $\widetilde{P}$ versus the distance $\tilde{d}$ for the asymmetry parameter $A = \frac{1}{2}$ and the coupling constant $\Xi = 100$. Solid line corresponds to MC data, dashed line to the present theory with the pressure obtained via the thermodynamic route and dash-and-dot line to the leading term of the VSC theory [52], see Eq. (6.1).

charged plates [52], given by

$$\widetilde{P}_{\mathrm{VSC}} = -\frac{1}{2}(1+A^2) + \frac{1}{2}(1-A^2)\coth\left(\frac{1-A}{2}\tilde{d}\right), \quad (6.1)$$

is represented by the dash-and-dot curve. The VSC theory gives reasonable values of the pressure only for small values of $\tilde{d}$ corresponding to the repulsive regime of the pressure.

The results for the half-space occupation parameter τ as the function of the distance $\tilde{d}$ for the coupling constant $\Xi = 100$ are presented in Fig. 3. As before, the MC data are represented by solid line and the results of the present theory by dashed line. The agreement of the theory and MC simulations is very good as well. The limiting $\eta \to 0$ and $\eta \to \infty$ values of τ satisfy the requirements (4.15). It is interesting that the plot of $\tau(\tilde{d})$ is not monotonous. For very small distances between the walls the numbers of counterions attached to the left and right walls are equal, then increasing the distance counterions migrate from the right to the left walls. The half-space occupation parameter is minimal when counterions maximally attach to the left wall. For larger d, beyond this minimum, counterions move to the right. For infinite d, counterions fully screen the surface charge of both plates.

The results for the pressure $\widetilde{P}$ and the half-space occupation parameter τ as the functions of the distance $\tilde{d}$ for the coupling constant $\Xi = 30$ are presented in Figs. 4 and 5, respectively. The agreement of the theory and MC simulations is very good also for this value of Ξ.

Let us now discuss the asymptotic large-distance behavior of the pressure $\widetilde{P}$ observed in MC simulations. For large values of the coupling constant Ξ, there is an apparent scaling regime for the *attractive* $\widetilde{P} < 0$ in the region of large (but not too large) distances as predicted by the relations (4.42) and (4.43). At the same time, the PB regime (4.40) of the *repulsive* $\widetilde{P} > 0$

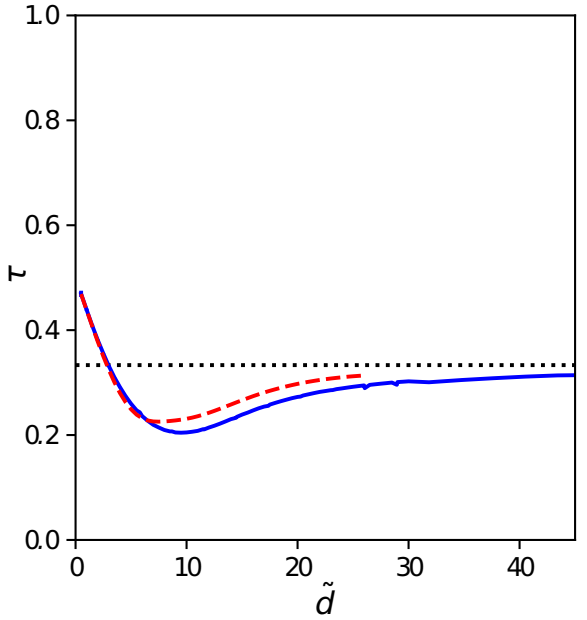

FIG. 3. The half-space occupation parameter τ versus the distance $\tilde{d}$ for the asymmetry parameter $A = \frac{1}{2}$ and the coupling constant $\Xi = 100$. Solid line corresponds to MC data and dashed line to the present theory. The horizontal dotted line shows the large-distance asymptotics as given by Eq. (4.15), yielding here $\tau = \frac{1}{3}$.

takes place at extremely large distances which are usually not accessible to standard MC simulations due to the lack of accuracy. The scaling region for the attractive $\widetilde{P}$ becomes less pronounced when decreasing Ξ and it even disappears for small values of Ξ. As concerns the scaling PB region for the repulsive $\widetilde{P}$, it moves down to smaller distances when decreasing Ξ and for small values of Ξ it is readily accessible by using standard MC simulations.

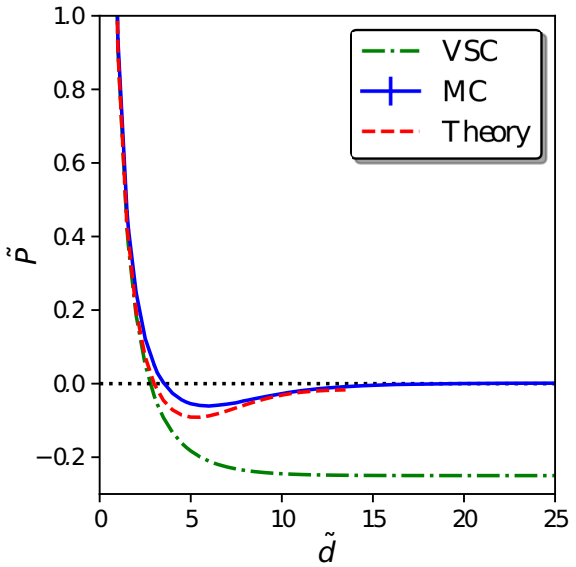

FIG. 4. The pressure $\widetilde{P}$ versus the distance $\tilde{d}$ for the asymmetry parameter $A = \frac{1}{2}$ and the coupling constant $\Xi = 30$. The notation is the same as in Fig. 2.

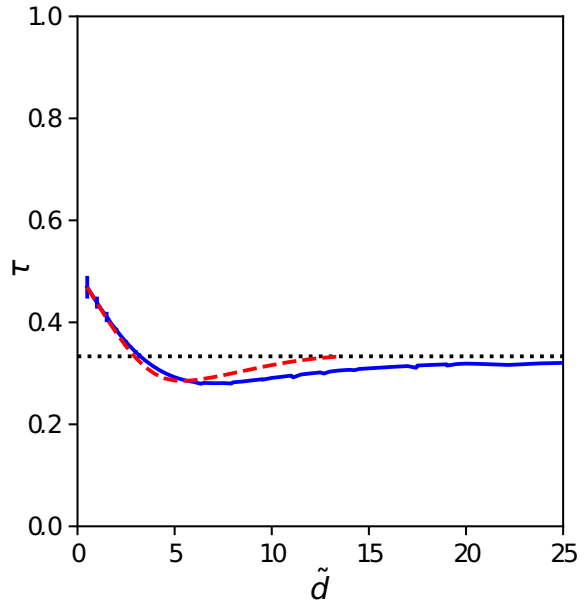

FIG. 5. The half-space occupation parameter τ versus the distance $\tilde{d}$ for the asymmetry parameter $A = \frac{1}{2}$ and the coupling constant $\Xi = 30$. The notation is the same as in Fig. 3.

To be more particular, the log-log plot of the absolute value of the pressure $|\widetilde{P}|$ versus the distance η for the coupling constant $\Xi = 300$ is pictured in Fig. 6. MC data are represented by open symbols (circles) for repulsive forces (pressures) and filled ones for attractive forces. The vacuum gap is here $800\,\mu$ units. Dotted line is the theoretical prediction of the

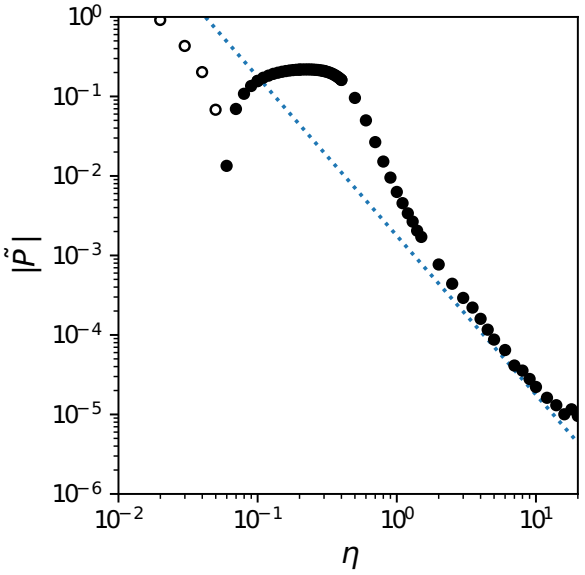

FIG. 6. The log-log plot of the absolute value of the pressure $|\widetilde{P}|$ versus the distance η for the coupling constant $\Xi = 300$. MC data are represented by open/filled circles for repulsive/attractive forces. The theoretical prediction of the asymptotic behavior (6.2) is represented by dotted line.

asymptotic behavior of the attractive pressure

$$\widetilde{P}_{\rm th} \sim -0.00177046... \frac{1}{\eta^2} \tag{6.2}$$

obtained from the relations (4.42) and (4.43) taken at $A = \frac{1}{2}$ and $\Xi = 300$. The agreement between MC data and this prediction is remarkable. It is seen that for the coupling constant $\Xi = 300$ the scaling regime for the attractive pressure (6.2) starts at $\eta \approx 3$; where it stops is hard to judge, as we lose numerical precision (for the MC simulations) around $\eta = 10$ for this Ξ-value. We add that at the ground state characterized by $\Xi \to \infty$, the asymptotic behavior of the pressure for $A = \frac{1}{2}$ takes the form with a quite distinct (almost doubled) prefactor:

$$\widetilde{P}_{\rm th} \sim -0.00352357... \frac{1}{\eta^2}. \tag{6.3}$$

VII. CONCLUSION

In the context of the effective interaction between symmetrically charged parallel plates mediated by counterions, it was shown in Ref. [40] that the effective fields created at zero temperature by the plate surface charges and the lattice structures of counterions on the plates are also relevant at nonzero temperatures, and rule the density profiles (hence also rule the pressure). The present work extends this effective-field method to asymmetrically charged plates. The technical complication in the asymmetric problem comes from the fact that each plate as a whole (i.e., the surface charge density plus the cloud of counterions attached to that plate) is not neutral. This causes stronger long-ranged interaction effects between the plates and requires the introduction of an additional (occupation) order parameter p (2.6) into the theory. This parameter is defined unambiguously in the ground state (counterions stuck on the plate surfaces) and its value is determined variationally to ensure the minimum of the energy (3.12). At nonzero temperatures, the order parameter p represents an auxiliary variational quantity which ensures the minimum of the free energy (4.38). Since at $T > 0$ the order parameter p cannot be measured in MC simulations, we have introduced the half-space occupation parameter τ (4.11) whose values are available in simulations. The theoretical results for the dimensionless pressure $\widetilde{P}$ and the half-space occupation parameter τ agree very well with MC data, for the intermediate coupling constant $\Xi = 100$ (see Figs. 2 and 3) as well as $\Xi = 30$ (see Figs. 4 and 5). By construction, our treatment improves in accuracy when Ξ is increased. It becomes exact for $\Xi \to \infty$.

An interesting result following from the present work deals with the asymptotic scaling behavior of the attractive pressure. It is known that at nonzero temperatures the pressure is repulsive at asymptotically large distances between the plates and takes the universal (i.e., independent of the like surface charge densities on the plates) Poisson-Boltzmann (PB) form (4.40). On the contrary, the asymptotic pressure is attractive at zero temperature, see the nonuniversal formula (3.39) which contains the Madelung constant of the hexagonal structure c and the asymmetry parameter A. The attraction phenomenon exists also for nonzero temperatures where two regions of large distances exist: *extremely* large distances at which the repulsive PB pressure (4.40) takes place and large distances at which the attractive pressure prevails, with the finite-Ξ correction in the nonuniversal prefactor given by Eqs. (4.42) and (4.43). We are thus in the situation of an intermediate asymptotics. The MC data of the pressure versus distance for the coupling constant $\Xi = 300$ in Fig. 6 are in perfect agreement with our theoretical prediction represented by dotted line. Of course, going to higher temperatures the full region of the attractive pressure diminishes and finally disappears for high enough temperatures.

Since the present method relies on the effective fields acting in the ground state, it is applicable to the region of large coupling constants Ξ. The fact that it provides reasonable results for the pressure $\widetilde{P}$ and half-space occupation parameter τ for a coupling constant Ξ as small as 30, see Figs. 4 and 5, is rather surprising. It would be useful to establish a theory covering both $\Xi \to \infty$ and $\Xi \to 0$ limits, to see the mutual interconnection and the corresponding ranges of the attractive and repulsive scaling regions of the pressure. A possible candidate is the SC method based on the idea of correlation holes substituting the Wigner crystal of counterions [39].

ACKNOWLEDGMENTS

We acknowledge useful discussions with Ivan Palaia. L.Š. is grateful to LPTMS for hospitality. The support of L.Š. received from Science Grant Agency (VEGA) Grant No. 2/0089/24 and Project No. APVV-20-0150 is acknowledged. M.T. thanks the Swedish Research Council for financial support (Grant No. 2021-04997).

APPENDIX A: PHASE I_p

The energy of phase I_p with commensurate values of $p \in \{1/2, 1/3, 1/4, 1/7, 1/9, \cdots\}$ is given by [49]

$$\frac{E_{\mathrm{I}_p}(\eta, p)}{Ne^2\sqrt{\sigma_L + \sigma_R}} = 2^{3/2}\pi\eta\left(p - \frac{A}{1+A}\right)^2 + c + \frac{p}{\sqrt{2}}[-\mathcal{K}(\eta) + \sqrt{p}\mathcal{K}(\sqrt{p}\eta)], \tag{A1}$$

where

$$\mathcal{K}(\eta) = \frac{1}{\sqrt{\pi}}\int_0^\infty \frac{dt}{\sqrt{t}}(1 - e^{-\eta^2 t})\left\{\left[\theta_3(e^{-\sqrt{3}t})\theta_3(e^{-t/\sqrt{3}}) - 1 - \frac{\pi}{t}\right] + \left[\theta_2(e^{-\sqrt{3}t})\theta_2(e^{-t/\sqrt{3}}) - \frac{\pi}{t}\right]\right\}. \tag{A2}$$

Introducing the generalized Misra functions

$$z_\nu(x, y) = \int_0^{1/\pi} \frac{dt}{t^\nu} e^{-xt} e^{-y/t}, \tag{A3}$$

in terms of the functions

$$I_2(x,y) = 2\sum_{j=1}^{\infty}(-1)^j\left[z_{3/2}\left(x, y+\sqrt{3}j^2\right) + z_{3/2}\left(x, y+\frac{j^2}{\sqrt{3}}\right)\right] + 4\sum_{j,k=1}^{\infty}(-1)^{j+k} z_{3/2}\left(x, y+\sqrt{3}j^2+\frac{k^2}{\sqrt{3}}\right),$$

$$I_3(x,y) = 2\sum_{j=1}^{\infty}\left[z_{3/2}\left(x, y+\sqrt{3}j^2\right) + z_{3/2}\left(x, y+\frac{j^2}{\sqrt{3}}\right)\right] + 4\sum_{j,k=1}^{\infty} z_{3/2}\left(x, y+\sqrt{3}j^2+\frac{k^2}{\sqrt{3}}\right) - \pi z_{1/2}(x,y),$$

$$I_4(x,y) = 4\sum_{j,k=1}^{\infty} z_{3/2}\left(x, y+\sqrt{3}(j-1/2)^2+\frac{(k-1/2)^2}{\sqrt{3}}\right) - \pi z_{1/2}(x,y), \tag{A4}$$

$\mathcal{K}(\eta)$ can be expressed as

$$\mathcal{K}(\eta) = \frac{1}{\sqrt{\pi}}[I_2(0,0) - I_2((\pi\eta)^2,0) + 2I_3(0,0) - I_3((\pi\eta)^2,0) - I_3(0,\eta^2) + I_4(0,0) - I_4(0,\eta^2)]. \tag{A5}$$

APPENDIX B: PHASE V_p

The energy of phase V_p with commensurate values of $p \in \{1/2, 1/4, 1/5, 1/8, 1/10, \cdots\}$ is given by [49]

$$\frac{E_{V_p}(\eta,p)}{Ne^2\sqrt{\sigma_L+\sigma_R}} = 2^{3/2}\pi\eta\left(p-\frac{A}{1+A}\right)^2 + c[(1-p)^{3/2}+p^{3/2}] + J(\eta,p), \tag{B1}$$

where

$$J(\eta,p) = p\sqrt{1-p}\frac{1}{2^{3/2}\sqrt{\pi}}\int_0^{\infty}\frac{dt}{\sqrt{t}}[-e^{-\eta^2(1-p)t} + \sqrt{3}e^{-3\eta^2(1-p)t}]$$
$$\times\left\{\left[\theta_3(e^{-\sqrt{3}t})\theta_3(e^{-t/\sqrt{3}}) - 1 - \frac{\pi}{t}\right] + \left[\theta_2(e^{-\sqrt{3}t})\theta_2(e^{-t/\sqrt{3}}) - \frac{\pi}{t}\right]\right\}. \tag{B2}$$

The first term on the right-hand side of Eq. (B1) corresponds to the Coulomb energy due to the nonneutrality of plate's entities.

[1] E. Raspaud, M. da Conceicao, and F. Livolant, Phys. Rev. Lett. **84**, 2533 (2000).
[2] T. Palberg, M. Medebach, N. Garbow, M. Evers, A. B. Fontecha, H. Reiber, and E. Bartsch, J. Phys.: Condens. Matter **16**, S4039 (2004).
[3] M. Brunner, J. Dobnikar, H. H. von Grünberg, and C. Bechinger, Phys. Rev. Lett. **92**, 078301 (2004).
[4] Ph. Attard, Ad. Chem. Phys. **XCII**, 1 (1996).
[5] Y. Levin, Rep. Prog. Phys. **65**, 1577 (2002).
[6] R. Messina, J. Phys.: Condens. Matter **21**, 113102 (2009).
[7] N. Ben-Tal, J. Phys. Chem. **99**, 9642 (1995).
[8] B. Jönsson and J. Stahlberg, Colloid Surf. B **14**, 67 (1999).
[9] J.-P. Hansen and H. Löwen, Annu. Rev. Phys. Chem. **51**, 209 (2000).
[10] L. Belloni, J. Phys.: Condens. Matter **12**, R549 (2000).
[11] A. Y. Grosberg, T. T. Nguyen, and B. I. Shklovskii, Rev. Mod. Phys. **74**, 329 (2002).
[12] G. L. Gouy, J. Phys. Theor. Appl. **9**, 457 (1910).
[13] D. L. Chapman, London, Edinburgh, Dublin Philos. Mag. J. Sci. **25**, 475 (1913).
[14] Within Poisson-Boltzmann theory, surfaces with surface potentials of the same sign may attract, while surfaces with opposite surface charges may repel, at short enough distances [15]. Yet, for surface charges of the same sign, Poisson-Boltzmann yields repulsion. This is the situation we investigate in this work.
[15] D. Chan, T. W. Healy, and L. R. White, J. Chem. Soc., Faraday Trans. 1 **72**, 2844 (1976).
[16] B. V. Derjaguin, N. V. Churaev, and V. M. Muller, *Surface Forces* (Plenum Publishing, New York, NY, 1987).
[17] P. Attard, D. J. Mitchell, and B. W. Ninham, J. Chem. Phys. **88**, 4987 (1988).
[18] R. Podgornik, J. Phys. A: Math. Gen. **23**, 275 (1990).
[19] R. R. Netz and H. Orland, Eur. Phys. J. E **1**, 203 (2000).
[20] L. Gulbrand, B. Jönsson, H. Wennerström, and P. Linse, J. Chem. Phys. **80**, 2221 (1984).
[21] R. Kjellander and S. Marčelja, Chem. Phys. Lett. **112**, 49 (1984).
[22] N. Grønbech-Jensen, R. J. Mashl, R. F. Bruinsma, and W. M. Gelbart, Phys. Rev. Lett. **78**, 2477 (1997).
[23] A. Khan, B. Jönsson, and H. Wennerström, J. Phys. Chem. **89**, 5180 (1985).
[24] R. Kjellander, S. Marčelja, and J. P. Quirk, J. Colloid Interface Sci. **126**, 194 (1988).
[25] V. A. Bloomfield, Biopolymers **31**, 1471 (1991).
[26] P. Kékicheff, S. Marčelja, T. J. Senden, and V. E. Shubin, J. Chem. Phys. **99**, 6098 (1993).
[27] M. Dubois, T. Zemb, N. Fuller, R. P. Rand, and V. A. Pargesian, J. Chem. Phys. **108**, 7855 (1998).
[28] A. G. Moreira and R. R. Netz, Europhys. Lett. **52**, 705 (2000).
[29] A. G. Moreira and R. R. Netz, Phys. Rev. Lett. **87**, 078301 (2001).

[30] R. R. Netz, Eur. Phys. J. E **5**, 557 (2001).
[31] M. Kanduč and R. Podgornik, Eur. Phys. J. E **23**, 265 (2007).
[32] D. S. Dean, R. R. Horgan, A. Naji, and R. Podgornik, J. Chem. Phys. **130**, 094504 (2009).
[33] A. Naji and R. R. Netz, Phys. Rev. Lett. **95**, 185703 (2005).
[34] Y. Levin, J. J. Arenzon, and J. F. Stilck, Phys. Rev. Lett. **83**, 2680 (1999).
[35] B. I. Shklovskii, Phys. Rev. E **60**, 5802 (1999).
[36] L. Šamaj and E. Trizac, Phys. Rev. Lett. **106**, 078301 (2011).
[37] L. Šamaj and E. Trizac, Phys. Rev. E **84**, 041401 (2011).
[38] L. Šamaj, A. P. dos Santos, Y. Levin, and E. Trizac, Soft Matter **12**, 8768 (2016).
[39] I. Palaia, M. Trulsson, L. Šamaj, and E. Trizac, Mol. Phys. **116**, 3134 (2018).
[40] I. Palaia, A. Goyal, E. Del Gado, L. Šamaj, and E. Trizac, J. Phys. Chem. B **126**, 3143 (2022).
[41] S. Earnshaw, Trans. Camb. Phil. Soc. **7**, 97 (1842).
[42] G. Goldoni and F. M. Peeters, Phys. Rev. B **53**, 4591 (1996).
[43] J.-J. Weis, D. Levesque, and S. Jorge, Phys. Rev. B **63**, 045308 (2001).
[44] R. Messina and H. Löwen, Phys. Rev. Lett. **91**, 146101 (2003).
[45] V. Lobaskin and R. R. Netz, Europhys. Lett. **77**, 38003 (2007).
[46] E. C. Oğuz, R. Messina, and H. Löwen, Europhys. Lett. **86**, 28002 (2009).
[47] L. Šamaj and E. Trizac, Phys. Rev. B **85**, 205131 (2012).
[48] M. Antlanger, G. Kahl, M. Mazars, L. Šamaj, and E. Trizac, Phys. Rev. Lett. **117**, 118002 (2016).
[49] M. Antlanger, G. Kahl, M. Mazars, L. Šamaj, and E. Trizac, J. Chem. Phys. **149**, 244904 (2018).
[50] B. Hartl, M. Mihalkovič, L. Šamaj, M. Mazars, E. Trizac, and G. Kahl, J. Chem. Phys. **159**, 204112 (2023).
[51] L. Šamaj, M. Trulsson, and E. Trizac, Phys. Rev. E **102**, 042604 (2020).
[52] M. Kanduč, M. Trulsson, A. Naji, Y. Burak, J. Forsman, and R. Podgornik, Phys. Rev. E **78**, 061105 (2008).
[53] M. Z. Bazant, K. Thornton, and A. Ajdari, Phys. Rev. E **70**, 021506 (2004).
[54] D. Henderson and L. Blum, J. Chem. Phys. **69**, 5441 (1978).
[55] D. Henderson, L. Blum, and J. L. Lebowitz, J. Electroanal. Chem. Interfacial Electrochem. **102**, 315 (1979).
[56] S. L. Carnie and D. Y. C. Chan, J. Chem. Phys. **74**, 1293 (1981).
[57] H. Wennerström, B. Jönsson, and P. Linse, J. Chem. Phys. **76**, 4665 (1982).
[58] Y. G. Chen and J. D. Weeks, Proc. Natl. Acad. Sci. USA **103**, 7560 (2006).
[59] C. D. Santangelo, Phys. Rev. E **73**, 041512 (2006).
[60] A. P. dos Santos, A. Diehl, and Y. Levin, J. Chem. Phys. **130**, 124110 (2009).
[61] I.-C. Yeh and M. L. Berkowitz, J. Chem. Phys. **111**, 3155 (1999).
[62] M. Mazars, J.-M. Caillol, J.-J. Weis, and D. Levesque, Condens. Matter Phys. **4**, 697 (2001).